

Diffusion-Driven Universal Model Inversion Attack for Face Recognition

Hanrui Wang^{1,*}, Shuo Wang², Chun-Shien Lu³, and Isao Echizen¹

¹National Institute of Informatics, Japan; ²Shanghai Jiao Tong University, China; ³Academia Sinica, Taiwan

*Corresponding Author

{hanrui_wang, iechizen}@nii.ac.jp, wangshuosj@sjtu.edu.cn, lcs@iis.sinica.edu.tw

Abstract—Facial recognition technology poses significant privacy risks, as it relies on biometric data that is inherently sensitive and immutable if compromised. To mitigate these concerns, face recognition systems convert raw images into embeddings, traditionally considered privacy-preserving. However, model inversion attacks pose a significant privacy threat by reconstructing these private facial images, making them a crucial tool for evaluating the privacy risks of face recognition systems. Existing methods usually require training individual generators for each target model, a computationally expensive process. In this paper, we propose DiffUMI, a training-free diffusion-driven universal model inversion attack for face recognition systems. DiffUMI is the first approach to apply a diffusion model for unconditional image generation in model inversion. Unlike other methods, DiffUMI is universal, eliminating the need for training target-specific generators. It operates within a fixed framework and pretrained diffusion model while seamlessly adapting to diverse target identities and models. DiffUMI breaches privacy-preserving face recognition systems with state-of-the-art success, demonstrating that an unconditional diffusion model, coupled with optimized adversarial search, enables efficient and high-fidelity facial reconstruction. Additionally, we introduce a novel application of out-of-domain detection (OODD), marking the first use of model inversion to distinguish non-face inputs from face inputs based solely on embeddings.

I. INTRODUCTION

A. Background

Face recognition technology presents significant privacy risks, as it involves processing biometric data that is both sensitive and immutable if compromised. Modern systems address these concerns by leveraging feature embedding techniques, which enhance scalability, generalization to unknown identities, and retrieval efficiency [1], [2], [3], [4]. These systems transform facial images into feature embeddings, facilitating recognition through distance-based metrics such as cosine similarity or Euclidean distance. This kind of approaches was traditionally considered privacy-preserving, as it encodes raw biometric data [5], [6], as shown in Fig. 1.

However, model inversion attacks present a significant privacy threat by reconstructing facial images solely from feature embeddings, as illustrated in Fig. 1. These reconstructions can facilitate further security breaches, including presentation attacks such as spoofing via photo, video replay, or 3D mask techniques [7]. As a result, model inversion attacks are essential for assessing the privacy vulnerabilities of face recognition systems [8].

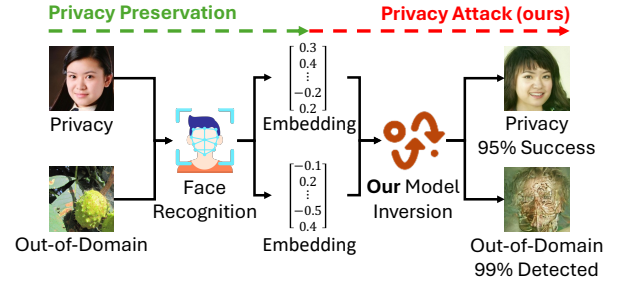


Fig. 1. Applications of our diffusion-driven universal model inversion (DiffUMI) for privacy attacks and out-of-domain detection (OODD). DiffUMI reconstructs images solely from embeddings, previously considered privacy-preserving, achieving 94.72% reconstruction success for face inputs, with reconstructions closely matching the target identity. Additionally, our OODD framework detects 98.9% of non-face inputs with a 3.9% error rate in misclassifying face inputs, demonstrating its robustness in distinguishing in-domain from out-of-domain data.

Nevertheless, existing model inversion attacks face several critical challenges. As summarized in Tab. I, most approaches are training-dependent, requiring the training or fine-tuning of a target-specific generator for each attack, which incurs significant computational costs [10], [12], [11], [17], [14], [15], [16], [18], [13], [19], [20], [21], [22]. Additionally, embedding-based face recognition models are designed to generalize to unknown identities, making feature extraction an open-set task that accommodates a wide range of inputs, including those not seen during the training of the face recognition model or the generator used for inversion. This open-set nature necessitates that model inversion attacks generalize to an infinite number of identities, a requirement many existing methods fail to meet [9], [11], [17], [14], [15], [16], [18], [20], [23], [24], [26].

Another major challenge is ensuring high visual fidelity in reconstructed images. To effectively retrieve identity-related privacy, model inversion requires high-resolution reconstructions rich in visual attributes. A full headshot-style reconstruction, *a.k.a.* selfie, represents the optimal granularity for identity recovery [19], [25], [21], [22], [23], [26]. However, due to prohibitive training costs, most existing methods generate low-resolution reconstructions (*e.g.*, 64×64 or grayscale images) and often focus only on the facial region, which may lack sufficient perceptual detail for accurate human identity recognition [9], [10], [12], [11], [17], [14], [15], [16], [18],

TABLE I
OVERVIEW OF RELATED WORKS ON MODEL INVERSION ATTACKS.

Method	Generator	Training-Free ¹	Attack Cost		Query ³	Task		Visual Fidelity		Code
			Input	W/B ²		Open-Set ⁴	OODD ⁵	Resolution ⁶	Selfie ⁷	
MIA [9] [2015]	None	✓	Label	Both	N/D	✗	✗	GrayScale	✗	✓
NbNet [10] [2018]	DeconvNet	✗	Embedding	Black	19.2M	✓	✗	RGB160	✗	✓
Amplified-MIA [11] [2023]	DeconvNet	✗	Label	Black	30K	✗	✗	GrayScale64	✗	✓
DSCasConv [12] [2024]*	DeconvNet	✗	Embedding	White	6.4M	✓	✗	RGB112	✗	✓
DiBiGAN [13] [2020]	C-GAN	✗	Embedding	Both	490K	✓	✗	RGB	✗	✗
GMI [14] [2020]	C-GAN	✗	Label	White	182K	✗	✗	RGB64	✗	✓
α -GAN [15] [2022]	C-GAN	✗	Label	White	N/D	✗	✗	GrayScale	✗	✗
PLG-MI [16] [2023]	C-GAN	✗	Label	White	N/D	✗	✗	RGB64	✗	✓
LOKT [17] [2023]	C-GAN	✗	Label	Black	N/D	✗	✗	RGB128	✗	✓
ABE-MI [18] [2025]	C-GAN	✗	Label	Black	6K	✗	✗	RGB128	✗	✗
ID3PM [19] [2023]	C-Diffusion	✗	Embedding	Black	69K	✓	✗	RGB64	✓	✗
CDM [20] [2024]	C-Diffusion	✗	Label	Black	N/D	✗	✗	RGB64	✗	✗
Shahreza <i>et al.</i> [21] [2023]	StyleGAN	✗	Embedding	Both	70K	✓	✗	RGB1024	✓	✓
Shahreza <i>et al.</i> [22] [2024]*	StyleGAN	✗	Embedding	Both	25K	✓	✗	RGB1024	✓	✓
PPA [23] [2022]	StyleGAN	✓	Label	White	N/D	✗	✗	RGB1024	✓	✓
IF-GMI [24] [2024] ⁸	StyleGAN	✓	Label	White	N/D	✗	✗	RGB224	✗	✓
Dong <i>et al.</i> [25] [2023]	StyleGAN	✓	Embedding	Black	N/D	✓	✗	RGB1024	✓	✗
MAP ² V [8] [2024]*	StyleGAN	✓	Embedding	Both	6.9K	✓	✗	RGB192	✗	✓
PriDM [26] [2025]	DDPM	✓	Image	Black	N/D	✗	✗	RGB256	✓	✗
DiffUMI (ours)	DDPM	✓	Embedding	Both ⁹	(W)1.3K/(B)100K	✓	✓	RGB256	✓	✓

¹ “Training-Free” refers to methods where the generator is not target-specific, often pretrained on other tasks or not requiring a generator at all.

² White-box (W) model inversion attacks require access to the target model’s gradients, while black-box (B) attacks do not. “Both” indicates adaptability to both white-box and black-box settings.

³ N/D: Information not disclosed. Note that for other attacks, W/B = Both yields the same query cost in both settings.

⁴ Modern face recognition tasks inherently exhibit an “open-set” nature, allowing them to handle unknown identities that differ from the model’s training data. This requires attack methods capable of generalizing to an unbounded set of identities. Methods marked “No” are incompatible with open-set scenarios as they do not accept embeddings as inputs for model inversion.

⁵ Open-set face recognition inherently accommodates out-of-domain inputs. We propose the first OODD framework for explicitly detecting such inputs based solely on embeddings through model inversion techniques.

⁶ For example, “RGB160” refers to RGB images with a resolution of 160×160 pixels. An absence of a number indicates undisclosed resolution.

⁷ The reconstructed face varies in granularity, from isolated facial features to the full face or even the entire head (*e.g.*, a selfie, highest fidelity).

⁸ They define “OOD” as out-of-distribution, referring to a significant distributional shift between the face datasets used for training the target recognition model and the generator. This differs from our out-of-domain (OOD) definition, which describes instances such as a cat image in a face dataset.

⁹ DiffUMI achieves comparable reconstruction accuracy in both white-box and black-box settings, though the higher computational cost in the black-box setting limits its practical applicability.

* MAP²V is the most recent and relevant state-of-the-art benchmark aligned with our setting, both training-free and targeting open-set face recognition. Accordingly, we primarily compare against it under identical white-box conditions. Comparisons with attacks designed for closed-set face recognition are inapplicable due to differing assumptions: closed-set attacks rely on class labels, whereas we utilize target embeddings. Although DiffUMI also demonstrates superior performance over training-dependent attacks [22], [12] in Appendix A, they are not our primary baseline due to their critical limitation that each target model requires a separately trained generator, incurring significant computational overhead.

[13], [19], [20].

Finally, while diffusion models have gained prominence in modern generative AI research [27], generative adversarial networks (GANs) [28], [29], [30] remain the dominant paradigm for model inversion, as shown in Tab. I. This limited technological diversity restricts the application of state-of-the-art diffusion-driven generation techniques to model inversion. Existing diffusion-driven model inversion attacks typically rely on conditional diffusion (C-Diffusion) for facial image generation [19], [20], which are either inherently unsuitable for open-set face recognition or require significant computational resources, creating a trade-off between efficiency and image resolution (requiring 1.5 days [20] and 2 days [19] to train a generator restricted to 64×64 pixel resolution). The closest training-free diffusion-driven approach to ours is PriDM [26]; however, it requires masked facial images as inputs, which contain significantly more information than embeddings alone. Therefore, we classify PriDM as a face inpainting method

rather than a conventional model inversion technique.

B. Motivation

To address the aforementioned challenges, we propose **DiffUMI**, the first training-free, **Diffusion-driven Universal Model Inversion** attack. DiffUMI leverages a fixed, pretrained denoising diffusion model [31] for unconditional generation of full headshot-style selfies. Its universal nature arises from a consistent framework and generator that can adapt to any unknown identities and open-set face recognition models. DiffUMI eliminates the need for training target models or generators involving specific target identities, aligning with the open-set nature of face recognition and enhancing its suitability for open-set model inversion.

To achieve these objectives, we propose an algorithm that optimizes the diffusion model’s latent space via adversarial manipulation to refine reconstructions toward the target identity. We are the first to highlight the critical role of latent codes in generation fidelity and introduce an automated

selection method for reliable latent codes from randomly sampled Gaussian distributions. Additionally, we identify the risk of overfitting to the target model when editing latent space and address this with a novel ranked adversary strategy. We further reveal that fine-grained adversarial attacks [32], [33] are most effective in optimizing latent space without introducing excessive distortions. However, we acknowledge that fine-grained black-box adversarial manipulation for high-resolution generation (*e.g.*, $3 \times 256 \times 256$) is computationally expensive due to the high-dimensional latent space, posing a practical limitation for black-box diffusion-driven model inversion.

We evaluate DiffUMI using two widely used face datasets [34], [35] and four face recognition models [36], [37], [5], [6], comparing its performance to three benchmarks [8], [22], [12]. The results highlight DiffUMI’s superior attack effectiveness, showing that an unconditional diffusion model with optimized adversarial search enables efficient, high-fidelity facial reconstruction. For example, when DiffUMI targets the Labeled Faces in the Wild (LFW) dataset [35] and the ArcFace model [37] in the white-box setting, it achieves Type I and Type II accuracy of 98.55% and 94.72%, surpassing the benchmarks by 9.57% and 15.5%, respectively. Furthermore, we successfully breach privacy-preserving face recognition models [5], [6], which were specifically designed to resist model inversion, achieving Type II accuracies ranging from 84.42% to 92.87% across two face datasets, surpassing the benchmarks by 4.01% to 9.82%. This raises critical concerns about the adequacy of existing privacy-preserving techniques in mitigating such threats.

Moreover, we introduce a novel application of **Out-Of-Domain Detection (OODD)**, marking the first use of model inversion to distinguish non-face inputs from face inputs based solely on feature embeddings. As shown in Fig. 1, the open-set nature of face recognition models enables non-face inputs, such as those from ImageNet [38], to be processed into embeddings, which we define as out-of-domain inputs. These embeddings share the same dimensionality and numerical range as genuine facial images, making differentiation inherently challenging. We propose a novel OODD framework utilizing model inversion techniques, where reconstructions of out-of-domain inputs typically fail either by not resembling the target identity or by lacking discernible human facial features. These failure cases serve as key indicators for identifying potential out-of-domain inputs. Our OODD framework effectively detects 98.9% of non-face inputs [38] after embedding by the ArcFace model [37], with only a 3.9% error rate for genuine face inputs [34], [35]. These findings demonstrate the potential of model inversion in robust OODD and offer a fresh perspective on the relationship between model inversion and feature space interpretability.

Our key contributions are summarized as follows:

- We introduce DiffUMI, the first training-free, diffusion-driven universal model inversion attack, adaptable to any open-set face recognition model and unknown identities through a fixed framework and generator.

- We present the first analysis of latent code influence on generation fidelity and propose an automated method for selecting highly reliable latent codes from randomly sampled Gaussian distributions.
- We introduce a ranked adversary strategy to mitigate overfitting risks in latent space editing for generation. We demonstrate that fine-grained adversarial attack algorithms are particularly effective for manipulating the diffusion model’s latent space without introducing significant distortions or artifacts.
- We empirically establish DiffUMI as a state-of-the-art attack, revealing critical vulnerabilities in privacy-preserving face recognition systems and raising concerns about their ability to counter such threats.
- We introduce OODD, the first model inversion-based framework for distinguishing non-face inputs from face inputs based solely on feature embeddings.

II. UNIVERSAL MODEL INVERSION VIA DIFFUSION

This section introduces DiffUMI, outlining its objectives and framework in Sec. II-A. We then formalize the threat model and problem definition in Sec. II-B and Sec. II-C, respectively. Finally, we detail the algorithms for the three sequential steps in the framework, as presented in Sec. II-D through Sec. II-F. To make this paper self-contained, we outline the preliminaries of DDPM [39], face recognition, D’Agostino’s K^2 test [40], [41], [42], and MTCNN [43] in Appendix B. A comprehensive notation list with corresponding definitions is provided in Tab. XIII of Appendix C. The step-by-step algorithm of DiffUMI is detailed in Appendix D.

A. Overview

DiffUMI is introduced as a framework to assess the privacy risks of embedding-based face recognition models. A model is considered vulnerable if DiffUMI can reconstruct a facial image resembling the target identity using only its feature embedding. The primary goal of this privacy attack is to recover the target identity, rather than to precisely reconstruct the original image from which the embedding was derived.

To facilitate a universally applicable attack, DiffUMI employs a three-step attack mechanism, as depicted in Fig. 2. The framework utilizes DDPM [31], a denoising diffusion probabilistic model, as the generator. Unlike training-dependent model inversion attacks that require a generator to be trained for each target model, our generator is independently pre-trained for unconditional facial image synthesis from random Gaussian noise, rendering DiffUMI entirely training-free. As a result, DiffUMI facilitates effective attacks across diverse target identities and models without modifying any other components of the framework.

- *Step (a) (Preparation) – Latent Code Generation:* This phase independently generates a set of highly reliable latent codes, executed once, and applicable for attacking any target. The reliability of these latent codes is ensured by a selection strategy combining D’Agostino’s K^2 test [40], [41], [42] and MTCNN face detection [43]. The

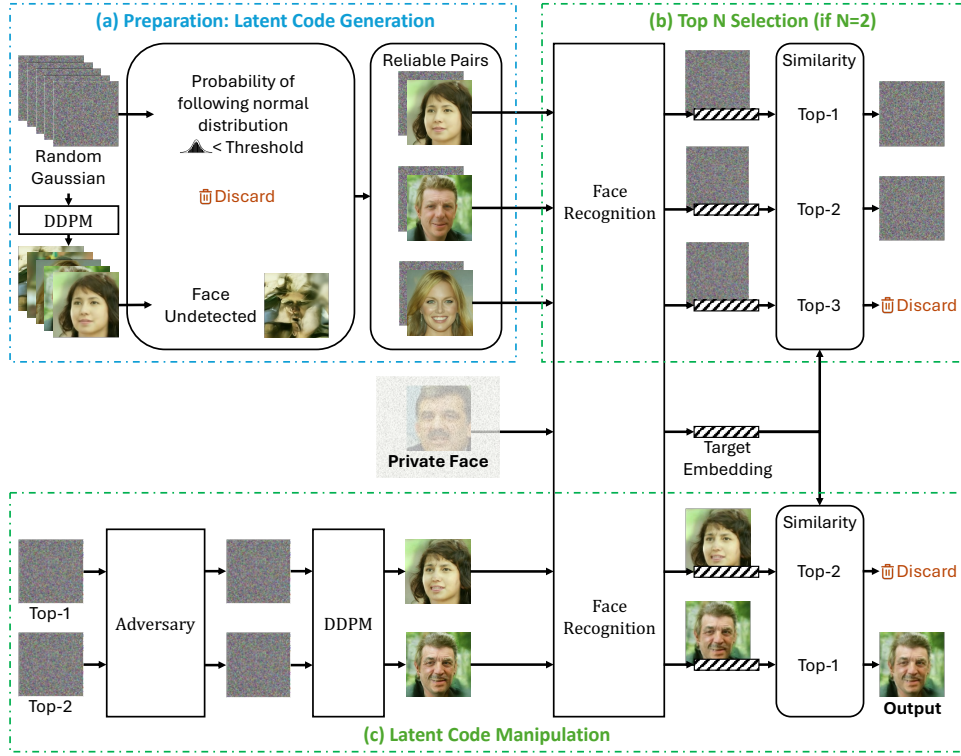


Fig. 2. Framework of DiffUMI, reconstructing a facial image with the same identity of a private face, solely from its embedding. The generator, a denoising diffusion model (DDPM) [31], is pretrained independently, without prior knowledge of the private face or the target model. In Step (a), a set of highly reliable latent codes is generated, executed only once, and applicable for attacks on any target. In Step (b), N latent codes are selected based on the reconstruction embeddings most similar to the target embedding, serving as initialization for Step (c). In Step (c), these latent codes undergo adversarial refinement to progressively align the reconstructions with the target embedding. The final output is the reconstruction with the highest embedding similarity to the target. Notably, despite initial rankings, a higher-ranked latent code may yield suboptimal reconstruction after adversarial manipulation.

K^2 test ensures the latent codes follow a normal distribution, improving statistical reliability, while MTCNN ensures that the generated images contain explicit facial features. Together, these criteria enhance the latent codes' robustness against subsequent adversarial manipulations, minimizing distortions and artifacts.

- *Step (b) – Top N Selection:* From the latent codes generated in Step (a), the top N are selected based on the embedding similarity between their reconstructions and the target embedding, as assessed by the target model. This ensures that the initial latent codes are well-aligned with the target identity, facilitating more effective adversarial manipulation in the next step.
- *Step (c) – Latent Code Manipulation:* The selected latent codes from Step (b) undergo iterative refinement through adversarial manipulation to progressively align their reconstructions with the target identity. The final output is the reconstruction exhibiting the highest embedding similarity to the target. To enhance efficiency, we introduce a ranked adversary strategy that leverages the rankings from Step (b) to optimize the order of latent code manipulation. Additionally, this strategy allows for early termination once the attack objective is met, thereby reducing computational overhead while maintaining effectiveness.

B. Threat Model

The proposed DiffUMI framework functions as an attacker, evaluating the privacy vulnerabilities of a target face recognition model. Specifically, it assesses whether a facial image reconstructed solely from an embedding generated by the model can accurately resemble the identity of the original face associated with that embedding.

Attack Knowledge: The attacker's knowledge is categorized based on access to the target model's gradients, in addition to utilizing the embedding for the privacy attack:

- *White-box:* The attacker has access to both the target embedding and the model's gradients.
- *Black-box:* The attacker only has access to the target embedding and can interact with the model via query-based feedback.

Attack Objective: Human assessment of privacy leakage, *i.e.*, whether the reconstructed facial image resembles the target identity, is subjective and varies across individuals. Therefore, we evaluate the attack's success using face recognition models, considering it successful if the reconstructed image is classified as the target identity.

Given that the attack process relies solely on the target embedding and model, there is a risk of overfitting due to adversarial artifacts rather than capturing true facial features.

To mitigate this, we evaluate the attack's success across multiple face recognition models, beyond just the target model. Formally, the attack objectives are as follows:

- *During attack:* The reconstructed facial image's embedding, when processed by the target model, achieves maximal similarity to the target embedding (see Sec. II-C).
- *During evaluation:* The reconstructed facial image is classified as the target identity by multiple face recognition models, even when compared with other images of the same identity, excluding the one corresponding to the target embedding (see Sec. IV).

C. Problem Definition and Objective Function

Given a target face x^T and the embedding function of a target model $F(\cdot)$, DiffUMI seeks to reconstruct $\hat{x} \approx x^T$ using only the feature embedding $z^T = F(x^T)$. However, in the context of privacy attacks, the goal is not for \hat{x} to be visually identical to x^T , but rather to share the same identity. Hence, the objective of DiffUMI is reformulated as:

$$F(\hat{x}) \approx F(x^T). \quad (1)$$

We define the reconstructed image \hat{x} , generated by applying a pretrained DDPM [31] as a generative function $G(\cdot)$ to an initial Gaussian noise sample x_G :

$$\hat{x} = G(x_G). \quad (2)$$

The generator operates on a latent code x_G of size $3 \times 256 \times 256$, sampled from a Gaussian distribution. Thus, Eq. (1) is reformulated as:

$$F(\hat{x}) = F(G(x_G)) \approx F(x^T). \quad (3)$$

Randomly sampled latent codes generally do not satisfy Eq. (3). To address this, we introduce an adversarial attack to manipulate the latent code:

$$x'_G = x_G + \delta, \quad \text{s.t.} \quad \|\delta\|_p \leq \epsilon, \quad (4)$$

where δ denotes the adversarial perturbation and ϵ is the perturbation magnitude constrained by the L_p -norm. The objective is then formulated as:

$$F(G(x_G + \delta)) \approx F(x^T), \quad (5)$$

where x_G is drawn from a random Gaussian distribution.

Eq. (5) is satisfied when the similarity measure exceeds a predefined threshold τ_F , indicating that the reconstructed image is classified as the same identity as the target. τ_F is a parameter of face recognition models, set at the minimum equal error rate for standard face recognition tasks using real facial images. While τ_F serves as a criterion for evaluating attack success by verifying whether the reconstruction matches the target, it is not involved in attack optimization or required as attack knowledge. The objective function \mathcal{L} of DiffUMI is formulated as:

$$\begin{aligned} \hat{z} &= F(\hat{x}) = F(G(x_G + \delta)), \\ z^T &= F(x^T), \\ \mathcal{L} &= S(\hat{z}, z^T) = \frac{\hat{z} \cdot z^T}{\|\hat{z}\| \|z^T\|}, \end{aligned} \quad (6)$$

where $S(\cdot, \cdot)$ denotes the function computing cosine similarity. DiffUMI aims to maximize \mathcal{L} by iteratively manipulating the latent code until:

$$\arg \max_{\hat{x}} \mathcal{L}. \quad (7)$$

D. Step (a) - Preparation: Latent Code Generation

We propose a two-stage approach for generating reliable latent codes as candidate initializations for DiffUMI (Fig. 14 of Appendix D). This strategy incorporates D'Agostino's K^2 test [40], [41], [42] to ensure that the selected latent codes conform to a normal distribution, referred to as Gaussian normality, and utilizes MTCNN [43] for face detection to guarantee that the generated latent codes produce discernible facial features.

The sequence of operations is deliberately structured: the K^2 test is performed first, followed by face detection. This ordering is chosen because generating a new random Gaussian template incurs minimal computational cost, though a significant portion may fail the K^2 test. Conversely, face detection is computationally more expensive, involving both image generation and verification. However, latent codes passing the K^2 test are more likely to meet the face detection criterion, thereby optimizing efficiency.

This phase independently generates a set of reliable latent codes, which can be used for attacking any target. Since it is executed only once, the K^2 test and face detection criteria can be applied rigorously to maximize the reliability of the generated latent codes.

1) Normality Test via D'Agostino's K-Square Statistic:

Reconstructing a facial image using DDPM requires a latent code of size $3 \times 256 \times 256$ that follows a normal distribution (*i.e.*, Gaussian normality) [31]. The adherence of randomly generated latent codes to a normal distribution varies (Fig. 3) and generally correlates with reconstruction fidelity (higher is better). However, even initially high-normality codes degrade after manipulation (Eq. (4)), as demonstrated in Fig. 4. To mitigate this effect, we employ D'Agostino's K^2 test [40], [41], [42] to select latent codes with higher normality prior to manipulation, improving initial reconstruction quality and better preserving fidelity despite subsequent normality reduction.

Given a randomly generated latent code x_G , the K^2 test function $K(\cdot)$ [40], [41], [42] quantifies deviations from normality based on skewness and kurtosis, producing a probability value:

$$p_K = K(x_G). \quad (8)$$

Latent codes are selected via a normality threshold τ_K :

$$x_G \text{ is selected if } p_K \geq \tau_K, \quad (9)$$

where τ_K is chosen sufficiently large as generating a random Gaussian template remains computationally efficient. This selection process prioritizes latent codes closely adhering to Gaussian properties, enhancing robustness in subsequent steps.

2) *Face Detection via MTCNN:* We observe that randomly generated latent codes may fail to produce recognizable faces, as shown in Fig. 3 and Fig. 5. To ensure face presence in

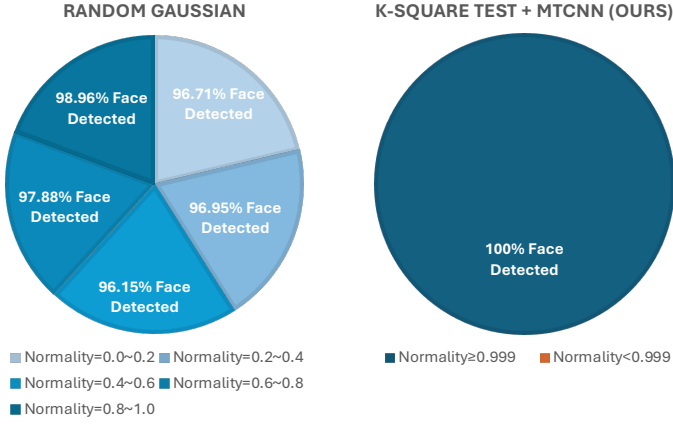


Fig. 3. Reliability of randomly generated latent codes and the proposed strategy. The face detection confidence threshold is set to $\tau_D = 0.99$. As shown in the left subfigure, the Gaussian normality of randomly generated latent codes fluctuates, with higher normality generally leading to improved face detection rates, as indicated by darker regions. Our strategy guarantees 100% Gaussian normality, with $p_K \geq 0.999$, and consistently achieves a 100% face detection rate, with $p_D \geq 0.99$.

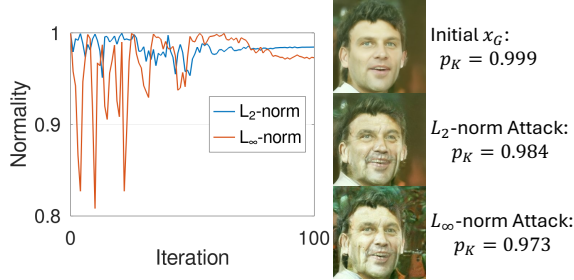


Fig. 4. Degradation of Gaussian normality due to adversarial manipulation. The L_2 -norm constrained adversary more effectively mitigates the decline in normality compared to the L_∞ -norm adversary, leading to enhanced reconstruction fidelity..

generated images, we utilize MTCNN [43], a deep learning-based face detection framework. Given a latent code x_G , we generate an image \hat{x} using DDPM $G(\cdot)$:

$$\hat{x} = G(x_G). \quad (10)$$

Next, we apply the detection function $D(\cdot)$ to assess face presence, yielding a confidence score p_D :

$$p_D = D(\hat{x}). \quad (11)$$

We define a threshold τ_D for high-confidence face detection:

$$(x_G, \hat{x}) \text{ is selected if } p_D \geq \tau_D, \quad (12)$$

where τ_D is set sufficiently high since most latent codes passing the K^2 test also meet the face detection criterion. This ensures that only images with strong facial feature likelihoods are retained for further processing. The reconstructed facial image \hat{x} and x_G are stored together to enhance efficiency in the subsequent top N latent code selection step.



Fig. 5. Failed face generation using randomly generated latent codes, where MTCNN fails to detect a face, resulting in a detection confidence of $p_D = 0$.

Target	Initial		Final	
Similarity \uparrow	0.2887	0.2831	0.9284	0.9817
Rank	Top-1	Top-2	Top-2	Top-1

Fig. 6. An example where the initial latent code, resulting in the optimal initial reconstruction, fails to yield the best outcome following adversarial manipulation.

E. Step (b) - Top N Latent Code Selection

In Step (a), DiffUMI generates a set of V randomly sampled yet reliable latent codes and their corresponding reconstructions $\{(x_{G_v}, \hat{x}_v)\}_{v=1}^V$. Instead of processing all V candidates, it may select the one with the highest initial embedding similarity to the target, expecting lowest computational costs and distortions. However, the latent code yielding the best initial reconstruction may not always produce the optimal result after adversarial manipulation (Fig. 6). To address this, DiffUMI refines selection by choosing the top N latent codes from V (Fig. 15 of Appendix D), where increasing N improves model inversion performance but incurs higher computational overhead.

In particular, the V reliable pairs are input into the target face recognition model, which outputs V feature embeddings. Note that $\hat{x}_v = G(x_{G_v})$, previously computed and stored during Step (a) for face detection (Sec. II-D2), is used. Similarities, as described in Eq. (6), are calculated between these V embeddings and the target embedding. The top N embeddings, exhibiting the highest similarity, are retained for Step (c) as the initial latent codes for adversarial manipulation.

In the black-box setting, as outlined in Sec. II-B, each of the (x_{G_v}, \hat{x}_v) pairs requires access to the target model, leading to a total of V queries in Step (b):

$$Q_{TopN} = V, \quad (13)$$

where V is the size of candidates from Step (a).

F. Step (c) - Latent Code Manipulation

As outlined in Sec. II-C, a randomly sampled latent code rarely satisfies the attack objective of reconstructing a facial image that shares the same identity as the target, even for the top-1 selection from Step (b). Therefore, refining the initial latent code is crucial to align the reconstructed face with the

target. Existing methods manipulate latent codes starting from either the top-1 code (as discussed in Sec. II-E) or a latent code fusion of the top N selections [8]. However, we observe that fusing reduces similarity significantly compared to the top-1 or top-2 selections. Additionally, relying on a single fused initialization may fail to ensure effective reconstruction, akin to the limitations of the top-1 approach. To overcome these challenges, we propose the *Ranked Adversary* method, which retains the top N selection strategy while prioritizing latent codes with higher similarity for earlier adversarial manipulation. This approach introduces early termination when the attack objective is met, optimizing computational efficiency while preserving effectiveness.

1) *Algorithm of Ranked Adversary*: The Ranked Adversary approach (Fig. 16 of Appendix D) initiates the refinement process with the top-1 latent code x_{G_1} , applying an adversarial attack strategy to iteratively adjust x_{G_1} in pursuit of the objective defined in Eq. (7), guided by the objective function in Eq. (6). The process concludes when the similarity measure \mathcal{L}_1 exceeds the predefined attack threshold τ_A , indicating successful manipulation where the reconstructed image sufficiently matches the target. In such cases, the reconstructed image $\hat{x}_1 = G(x_{G_1} + \delta_1)$ is produced as the final model inversion result. If \mathcal{L}_1 remains below τ_A after the maximum adversarial iterations t_{max} , the top-2 latent code x_{G_2} undergoes the same optimization process. If none of the top N latent codes achieve $\mathcal{L}_n \geq \tau_A$, $n = 1, \dots, N$, the reconstruction with the highest \mathcal{L}_n is selected as the final output.

As shown in Fig. 7, setting $\tau_A = \tau_F$ may ensure successful target matching, but only on the target model. Increasing τ_A beyond τ_F enhances robustness, particularly on the test model. In contrast, excessively high τ_A or the absence of early stopping may lead to the attack proceeds beyond the point of achieving $\mathcal{L} > 0.98$, yielding negligible gains in optimization while exacerbating overfitting and diminishing generalization to the test model, as achieving such a threshold often forces adversarial manipulation to introduce artifacts that overfit the target model and exhaust all attack iterations. Therefore, we define τ_A for attacking the specific model as the maximum embedding similarity achievable by real facial images in this model, which represents the best case where, ideally, without any overfitting artifacts, the model can achieve the best similarity within the same identity. To compute this, we feed the entire face dataset \mathcal{X}_{real} (all real faces) into the target model, then compute the maximum similarity between any two images. The similarity between different identities is usually lower than that between the same identity. Thus, we define τ_A as follows:

$$\tau_A = \max S(F(x^i), F(x^j)), \quad x^i, x^j \in \mathcal{X}_{real}, \quad (14)$$

where $F(\cdot)$ is the embedding function of the target model, and $S(\cdot, \cdot)$ is the cosine similarity function.

2) *Adversarial Attack*: Ranked Adversary employs fine-grained adversarial attack algorithms, as defined by Wang *et al.* [33], utilizing APGD [32] in the white-box setting and GreedyPixel [33] in the black-box setting. While various

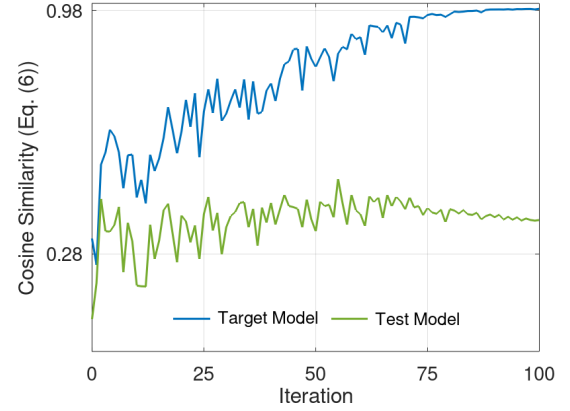


Fig. 7. Overfitting and inefficiency in objective function maximization (Eq. (6)) without the proposed ranked adversary strategy. The target model (in blue), PartialFace [6], uses a predefined similarity threshold $\tau_F = 0.28$ (minimum equal error rate), where embedding similarity above τ_F indicates identity matching. The blue curve depicts the attack process with a maximum of 100 iterations and an attack threshold $\tau_A = 1$, effectively disabling the ranked adversary strategy due to the unattainable objective. The tick at 0.98 marks the highest embedding similarity typically observed between real facial images of the same identity (LFW [35]) under the PartialFace model, which we designate as the optimal τ_A to terminate the adversary, thereby preventing overfitting and reducing computational cost. ArcFace [37] is used to evaluate overfitting. Here, test model validation is solely for performance assessment. It cannot be incorporated into objective optimization, as the attack operates solely on the target embedding, without access to the original image or its embedding of the test model.

adversarial attack algorithms can be adapted for latent code manipulation within our framework, our empirical observation shows that only these fine-grained methods yield satisfactory reconstructions without introducing significant distortions or artifacts. This is due to the sensitivity of the diffusion model's latent space, where even small perturbations can notably degrade reconstruction quality.

Additionally, we evaluated two alternative black-box attacks: Square attack [44], which uses the same L_2 -norm constrained perturbation magnitude ϵ as APGD, and BruSLe attack [45], a pixel-wise attack like GreedyPixel that enforces sparsity constraints rather than directly constraining ϵ . However, both methods performed inferiorly compared to GreedyPixel, as detailed in Sec. V-B.

3) *Query Efficiency in the Black-Box Setting*: In the black-box setting, the query cost for latent code manipulation arises from calculating the loss values in Eq. (6), which requires querying the target model to obtain feature embeddings of the reconstructed images. As a result, the total query cost is proportional to the number of iterations performed during adversarial manipulation. The query cost for optimizing a single latent code is given by:

$$Q_{Adv} = t_{max}, \quad (15)$$

where t_{max} represents the upper limit on the number of adversarial attack iterations.

Since the Ranked Adversary framework processes up to N selected latent codes, the total query cost for the latent code

manipulation phase is bounded by:

$$t_{max} \leq Q_{Adv} \leq N \times t_{max}. \quad (16)$$

Including the query cost incurred during the top N latent code selection in Step (b) (Eq. (13)), the overall query complexity of DiffUMI is:

$$Q = Q_{TopN} + Q_{Adv}. \quad (17)$$

In practical black-box attack scenarios, a predefined query budget Q_{max} is often imposed as a hard constraint. Under this restriction, the maximum number of iterations per adversarial attack process must satisfy:

$$t_{max} = \lfloor \frac{Q_{max} - V}{N} \rfloor, \quad (18)$$

where $\lfloor \cdot \rfloor$ denotes the floor function, returning the largest integer not exceeding the input, and V represents the size of latent code set in Step (a) used to select the top N latent codes.

III. OUT-OF-DOMAIN DETECTION

Deep learning models map both in-domain and out-of-domain inputs to the same feature space, making it challenging to distinguish between them based solely on embeddings. For example, in a face recognition system, both a human face and a non-face object (e.g., a cat) produce embeddings with identical dimensions and numerical ranges, despite their semantic differences. To address this, we leverage the high-fidelity reconstruction capabilities of our model inversion framework to develop an application of OOD that identifies out-of-domain inputs based on their embeddings.

As illustrated in Fig. 8, two common failure cases arise in model inversion, sometimes concurrently. In-domain inputs, such as facial images, typically yield accurate, recognizable reconstructions. In contrast, out-of-domain inputs are more likely to exhibit at least one of these failure cases. Hence, we classify an input as out-of-domain if either failure is detected.

Case 1: Reconstruction fails to match the target input across all test models except the target model.

We define *Test Models* as those distinct from the target model. For instance, if the target model is FaceNet [36], alternative models like ArcFace, DCTDP, and PartialFace can serve as test models [37], [5], [6]. This failure case is assessed using test models because the reconstruction tends to overfit the target model, resulting in a successful match when evaluated on the target model alone.

Given an input image x and the embedding function $F(\cdot)$ of the target model, we aim to identify whether x is an out-of-domain input using its embedding $z = F(x)$. First, we apply DiffUMI to obtain the reconstruction \hat{x} :

$$\hat{x} = \arg \max_{\hat{x}} S(F(\hat{x}), F(x)). \quad (19)$$

Next, using M test models F_1, \dots, F_M , we determine whether \hat{x} matches x in these models:

$$OOD_1 = \begin{cases} \text{True,} & \text{if } \forall m \in \{1, \dots, M\}, \\ & S(F_m(\hat{x}), F_m(x)) < \tau_{F_m}, \\ \text{False,} & \text{otherwise.} \end{cases} \quad (20)$$

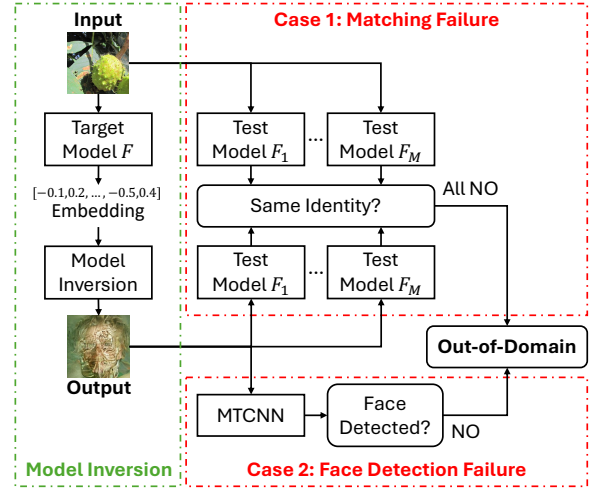


Fig. 8. The proposed out-of-domain detection (OODD) framework defines two failure scenarios in model inversion, both indicating out-of-domain inputs: (i) **Matching Failure**, where the reconstructed image fails to match the target input across all test models except the target model, and (ii) **Face Detection Failure**, where the reconstructed image lacks identifiable facial features.

where τ_{F_m} is the predefined similarity threshold, corresponding to the minimum equal error rate in face recognition.

Note that matching failure is defined only when the reconstruction fails to match the target across “all” test models (“ALL NO” in Fig. 8). Defining failure based on “any” mismatch, implying that an in-domain reconstruction should match the target across all test models, would be an overly idealized assumption, which consequently significantly increases the false detection of in-domain inputs as out-of-domain. For instance, our “all” strategy yields a 3.4% matching failure rate in detecting LFW [35] facial images on the FaceNet model [36], whereas the “any” criterion increases this error to 26.6%.

Case 2: The reconstruction lacks a detectable face, even if it matches the target input.

In this case, a successful match is likely attributable to adversarial artifacts rather than accurate identity reconstruction. We utilize MTCNN $D(\cdot)$ [43] with a detection threshold τ_D :

$$OOD_2 = \begin{cases} \text{True,} & \text{if } p_D = D(\hat{x}) < \tau_D, \\ \text{False,} & \text{otherwise.} \end{cases} \quad (21)$$

Here, τ_D may differ from the latent code generation threshold, as a higher τ_D in OODD increases false positives by classifying in-domain inputs as out-of-domain.

The final OODD decision is determined by the logical disjunction of both criteria: $OOD = OOD_1 \vee OOD_2$, where \vee represents the logical disjunction (OR) operator.

IV. EXPERIMENTAL SETTINGS

Face Recognition Models. We assess model inversion attacks on two widely used face recognition models, FaceNet [36] and ArcFace [37], and two privacy-preserving models, DCTDP [5] and PartialFace [6], which are designed to mitigate inversion attacks. The decision thresholds for all models are set at the minimum equal error rate, as outlined in Tab. II.

TABLE II
CONFIGURATION OF TARGET MODELS, WHITE-BOX DIFFUMI, AND OODD SETTINGS.

Face Recognition Model $F(\cdot)$	τ_F	Latent Code Generation (ours)			Latent Code Manipulation (ours)				€	OODD (ours) τ_D^1
		Volume V	τ_K	τ_D^1	Top N	t_{max}	τ_A	Norm		
FaceNet [36]	0.40	1,000	0.999	0.999	3	100	0.99	L_2	25	0.9933
ArcFace [37]	0.23						0.99		35	
DCTDP [5]	0.26						0.98		35	
PartialFace [6]	0.28						0.98		35	

¹ A higher detection confidence threshold is applied during latent code generation to ensure reliable initialization, as generating a random Gaussian template is computationally efficient.

Refer to Tab. XIII in Appendix C for notation definitions.

Datasets. We evaluate model inversion attacks and OODD using three datasets: LFW [35] and CelebA-HQ [34] for privacy attacks, and ImageNet [38], a non-face dataset, for OODD. Each dataset contains 1,000 samples. For LFW and CelebA-HQ, we select 10 images from each of 100 distinct identities for computing Type II accuracy. Datasets such as FFHQ [46], which lack identity annotations, are thus unsuitable. As our approach is training-free, large-scale datasets are unnecessary for evaluation.

LFW, which is independent of both face recognition model and generator training, serves as our primary evaluation dataset. In contrast, CelebA-HQ shares the training distribution of the generator but is not used to train any recognition models, enabling an assessment of whether such prior knowledge improves attack performance. The face recognition models themselves are trained on datasets distinct from both evaluation sets: FaceNet [36] and DCTDP [5] are trained on VGGFace2 [47], while ArcFace [37] and PartialFace [6] are trained on MS1MV2 [48].

Benchmark. We benchmark DiffUMI against MAP²V [8] in the white-box setting. As shown in Tab. I, MAP²V is the most recent and most relevant state-of-the-art baseline, sharing our training-free setup and focus on open-set face recognition. While DiffUMI also outperforms training-dependent attacks [22], [12], as detailed in Appendix A, they are not our primary baseline due to their limitation that each target model requires a separately trained generator, resulting in substantial computational overhead. We exclude closed-set face recognition attacks, as they rely on class labels rather than target embeddings, reflecting fundamentally different assumptions.

Experimental Setup. The configuration details for the white-box DiffUMI attack and OODD are provided in Tab. II, while the settings for the black-box DiffUMI attack are outlined in Fig. 10 of Sec. V-B. Specifically, τ_F is the cosine similarity threshold in face recognition, optimized to minimize the equal error rate. τ_K and τ_D in latent code generation are set close to the upper bound (1.0) to ensure highly reliable initialization. τ_A is defined in Eq. (14). For OODD, τ_D is set to maintain a maximum false positive rate of 5% for in-domain inputs. In the ablation studies, we vary one parameter at a time while holding all others constant. All experiments are conducted on an NVIDIA A100 40GB GPU.

Evaluation Protocols. Model inversion attacks and OODD are executed directly on the target model, often leading to

outputs that overfit this model. Consequently, exceptional performance on the target model may stem from adversarial artifacts rather than the accurate reconstruction of facial features, a scenario classified as a failure in Sec. III. To thoroughly evaluate the effectiveness of privacy attacks and OODD, we adopt the following evaluation protocols.

Type II Accuracy: Mai *et al.* [10] introduced Type I and Type II accuracy as metrics for evaluating the effectiveness of privacy attacks. In this study, we focus on Type II accuracy, which measures the similarity between reconstructed facial images and facial images from the target identity, but excluding the target facial image. This metric provides a more stringent evaluation by reducing the risk of overfitting to the target image, whose embedding serves as the reference during the attack process. Specifically, Type II accuracy is the rate at which the reconstructed image \hat{x} matches facial images $x^{j \neq T}$ from the target identity but different from the target face x^T :

Type II Accuracy =

$$\frac{\sum_{i=1}^I \sum_{j=1}^J \mathbb{I}\left(S(F(\hat{x}_i), F(x_i^{j \neq T})) \geq \tau_F\right)}{I}, \quad (22)$$

where $x_i^j \neq x_i^T$ but shares the same identity. $\mathbb{I}(\cdot)$ and $S(\cdot, \cdot)$ represent the indicator and cosine similarity functions, respectively. J denotes the number of other facial images associated with the identity of x_i^T , I is the total number of attack samples, and τ_F is the face recognition similarity threshold. A higher Type II accuracy reflects a stronger inversion attack from the attacker’s perspective and indicates greater vulnerability from the privacy protection standpoint.

For further validation, we also report Type I accuracy results in Appendix E, which reflect the strength of the inversion attack and highlight potential privacy vulnerabilities.

OODD Rate: The OODD rate quantifies the failure rate of model inversion, based on the two failure cases outlined in Sec. III. For in-domain inputs, a lower OODD rate is preferable, indicating fewer inversion failures. Conversely, for out-of-domain inputs, a higher OODD rate is desirable, reflecting improved detection performance.

Joint Evaluation Using Target and Test Models: Test models, as defined in Sec. III, refer to those that differ from the target model. Evaluating on these models helps mitigate overfitting to the target model. In this study, four face recognition models are utilized, with one designated as the target model and

TABLE III
TYPE II ACCURACY (%) OF DIFFUMI ACROSS FOUR FACE RECOGNITION MODELS.

Dataset	Target Model	Test Model				Avg.
		FaceNet	ArcFace	DCTDP	PartialFace	
CelebA	FaceNet	96.93	80.12	84.19	77.67	84.73
	ArcFace	92.76	99.06	94.23	92.84	94.72
	DCTDP	87.43	89.62	96.52	86.61	90.05
	PartialFace	80.06	87.29	85.82	96.14	87.33
LFW	FaceNet	98.56	66.23	73.31	59.92	74.51
	ArcFace	91.03	99.64	95.88	92.33	94.72
	DCTDP	90.34	95.37	99.44	86.31	92.87
	PartialFace	75.39	85.44	77.99	98.84	84.42

Gray cells indicate cases where the target and test models are identical. Green and Red highlight the most and least secure models, respectively, based on the lowest and highest Type II accuracy.

FaceNet [36] offers the strongest privacy protection, surpassing even the privacy-preserving PartialFace [6] and DCTDP [5], while ArcFace [37] provides the weakest.

the remaining three as test models for each attack. However, testing exclusively on test models may introduce bias, as the test models vary for each target model, leading to an unfair comparison of model vulnerability to privacy risks.

To address this, we adopt a joint evaluation approach that includes both the target and test models, ensuring consistent evaluation across all models. This approach mitigates the impact of overfitting to the target model alone.

Note that OOD is evaluated exclusively on test models, as detailed in Sec. III. This is because out-of-domain inputs can only be matched with their reconstruction (similar to Type I accuracy), and such matching is always successful on the target model due to overfitting.

V. PERFORMANCE

A. White-Box Model Inversion

We assess the vulnerability of face recognition models to privacy threats using DiffUMI in the white-box setting. As shown in Tab. III, all four models, including privacy-preserving variants, fail to prevent privacy leakage. DiffUMI achieves Type II accuracy between 74.51% and 94.72% across all models and datasets. Notably, the oldest standard model, FaceNet, demonstrates the highest resistance, highlighting the limitations of existing privacy-preserving techniques.

Compared to the benchmark, as shown in Tab. IV, DiffUMI consistently surpasses MAP²V in Type II accuracy and achieves similarity values closer to the attack threshold τ_A across all scenarios. The “random” rows represent unguided diffusion model generations, which fail to match targets, emphasizing the necessity of a structured inversion approach. The visualization in Fig. 9 further highlights DiffUMI’s superiority, demonstrating higher identity recovery accuracy than MAP²V. Our approach produces full headshot-style reconstructions, achieving optimal granularity for identity recovery.

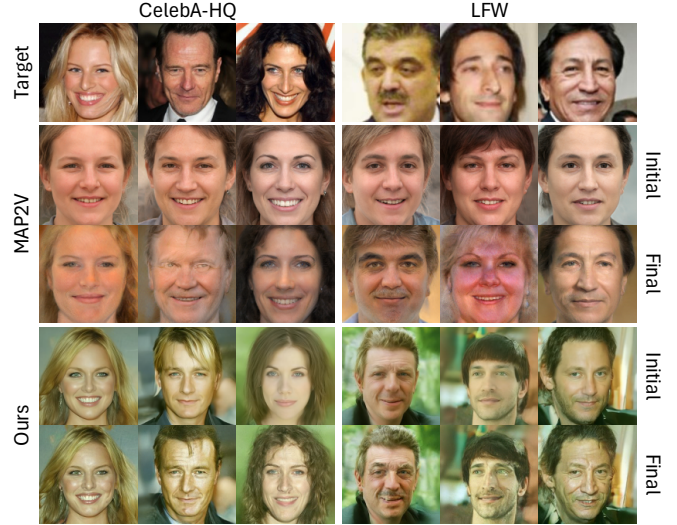


Fig. 9. Illustrations of DiffUMI generation versus MAP²V [8] in the white-box setting. DiffUMI achieves superior identity recovery accuracy, producing full headshot-style reconstructions that maximize identity granularity. “Initial” denotes pre-manipulation generations. The target model in this figure is the privacy-preserving PartialFace [6].

B. Black-Box Model Inversion

We evaluate DiffUMI in the black-box setting using various adversarial attack algorithms and compare its performance to the white-box counterpart. As shown in Fig. 10 (columns 3 vs. 10), black-box DiffUMI (GreedyPixel) achieves Type II accuracy comparable to its white-box version (APGD) but incurs substantially higher computational costs in time and queries. Due to these constraints, evaluations are conducted on only ten LFW samples [35] using the privacy-preserving PartialFace model [6], with efficiency improvements left for future work. Moreover, Fig. 10 (columns 4–6) demonstrates that only fine-grained attacks like GreedyPixel effectively manipulate diffusion model latent codes, whereas coarser black-box attacks (e.g., Square [44] and BruSLe [45]) fail. Comparing columns 6–10, increasing GreedyPixel’s query budget and sparsity allowance enhances model inversion accuracy by modifying more pixels but at a significantly higher computational cost.

C. Out-Of-Domain Detection

We evaluate the proposed OOD framework on both face and non-face datasets across four face recognition models. As shown in Fig. 11, the model inversion outputs for out-of-domain inputs primarily fall into the two failure cases described in Sec. III, each of which serves as an out-of-domain indicator within our framework. The results in Tab. V demonstrate a low detection rate for face datasets (LFW and CelebA-HQ) and a high detection rate for non-face inputs (ImageNet), validating the effectiveness of our detection.

D. Limited Impact of Prior Knowledge on Generator Training

We assess whether incorporating prior knowledge into the generator enhances reconstruction performance. To this end,

TABLE IV
PERFORMANCE OF OUR DIFFUMI ACROSS FOUR FACE RECOGNITION MODELS, COMPARED TO THE BENCHMARK ATTACK MAP²V [8].

Dataset	Attack	Target Model							
		FaceNet		ArcFace		DCTDP		PartialFace	
		Type II ³ (%) ↑	Similarity ⁴ ↑	Type II (%) ↑	Similarity ↑	Type II (%) ↑	Similarity ↑	Type II (%) ↑	Similarity ↑
CelebA	Original ¹	97.00	$\tau_A = 0.99$	99.09	$\tau_A = 0.99$	96.62	$\tau_A = 0.98$	95.65	$\tau_A = 0.98$
	Random ²	4.50	0.0822	1.73	0.0304	4.74	0.0771	9.72	0.1404
	MAP ² V	69.19	0.9248	84.61	0.8175	81.12	0.8135	80.84	0.7758
	Ours	84.73	0.9920	94.72	0.9898	90.05	0.9818	87.33	0.9818
LFW	Original ¹	98.60	$\tau_A = 0.99$	99.62	$\tau_A = 0.99$	99.47	$\tau_A = 0.98$	98.89	$\tau_A = 0.98$
	Random ²	0.91	0.0154	0.06	0.0046	0.09	0.0129	0.54	0.0568
	MAP ² V	73.14	0.9337	79.22	0.7723	83.05	0.7787	80.41	0.7636
	Ours	74.51	0.9917	94.72	0.9834	92.87	0.9774	84.42	0.9794

¹ Upper bound corresponding to true target faces.

² Lower bound referring to randomly generated facial images without a specific strategy.

³ Average Type II accuracy across four test models [37], [36], [5], [6], as per the joint evaluation using target and test models outlined in Sec. IV.

⁴ Cosine embedding similarity between target and reconstruction, computed in the target model, with values closer to τ_A indicating better performance.

Bold indicates the highest performance among attack methods, with our approach exceeding MAP²V attack by up to 15.54% in Type II accuracy.











Pre-Manipulation White-box Attack				Black-Box Attack					
1.Target	2.Top-1 Initial	3.APGD	4.Square	5.BruSLe	6.GreedyPixel	7.GreedyPixel	8.GreedyPixel	9.GreedyPixel	10.GreedyPixel
									
Magnitude ϵ	N/A	L2-norm $\epsilon = 35$	L2-norm $\epsilon = 35$	Unlimited	Unlimited	Unlimited	Unlimited	Unlimited	Unlimited
Sparsity	N/A	Unlimited	Unlimited	30%	10%	10%	10%	10%	Unlimited
Max. Queries	1,000	1,100	20,000	20,000	20,000	50,000	100,000	200,000	200,000
Similarity ↑	0.3086	0.9477	0.1088	0.6487	0.6817	0.7712	0.8266	0.8672	0.8794
Time Cost (H) ↓	0.01	0.05	11.04	11.05	3.78	9.91	15.24	38.38	39.11
Type II (%) ↑	0.0	78.9	1.1	32.2	41.1	67.8	76.7	80.0	81.1
OODD (%) ↓	90.0	10.0	100.0	40.0	30.0	10.0	10.0	10.0	10.0

Fig. 10. Performance of DiffUMI in the Black-Box Setting. Black-box DiffUMI achieves comparable reconstruction accuracy to its white-box counterpart (columns 3 vs. 10) in terms of Type II accuracy and OODD rate but incurs significantly higher computational costs in query complexity and runtime. Among black-box attack methods (columns 4-6), the fine-grained GreedyPixel algorithm, which introduces adversarial patterns akin to white-box attacks, is the only viable approach for manipulating diffusion model latent codes. Comparing columns 6-10, increasing the attack budget (query or sparsity) enhances model inversion accuracy but significantly raises computational costs. The target model is the privacy-preserving PartialFace [6], and the test model is ArcFace [37].



Fig. 11. Examples of two failure cases in the DiffUMI attack, which serve as indicators of OODD. The occurrence of either failure case signals an out-of-domain input: (i) **Matching Failure**, where the reconstructed image fails to align with the target input across all test models except the target model, and (ii) **Face Detection Failure**, where the reconstructed image lacks identifiable facial features. The target model in this figure is the privacy-preserving PartialFace [6].

TABLE V
OUT-OF-DOMAIN DETECTION RATE (%) ACROSS MODELS AND DATASETS.

Data	FaceNet	ArcFace	DCTDP	PartialFace
CelebA ↓	2.3	4.4	4.9	1.7
LFW ↓	4.9	3.4	3.7	1.4
ImageNet ↑	91.3	98.9	95.5	95.2

Our OODD framework achieves high detection rates for out-of-domain inputs while maintaining low error for in-domain inputs.

we train a DDPM on CelebA-HQ and attack target identities also drawn from CelebA-HQ (with disjoint identities), ensuring that the generator and target images share the same distribution. Results are compared against attacks on the LFW dataset. As shown in Tab. III and Tab. V, it is surprising that performance varies inconsistently between CelebA-HQ and LFW across both privacy attacks and OODD tasks. These findings indicate that, in training-free, open-set model inversion, prior knowledge of the data distribution has minimal impact on reconstruction accuracy. Even with shared distributions, the

TABLE VI
PERFORMANCE ACROSS DIFFERENT LATENT CODE RELIABILITIES.

Strategy	Time (s) ↓	Type II (%) ↑	OODD (%) ↓
Random Gaussian	290	82.78	3.1
K^2 Test	293	82.47	2.4
K^2 Test + MTCNN	256	84.42	1.4

Bold indicates the superiority of our strategy.

TABLE VII
PERFORMANCE (%) FOR VARYING VALUES OF N .

Top N	Time (s) ↓	Type II (%) ↑	OODD (%) ↓
1	189	81.06	1.9
3	256	84.42	1.4
5	289	85.21	0.9

Bold indicates the highest performance, showing that increasing N enhances reconstruction accuracy but increases computational cost.

generator cannot reliably synthesize identity-consistent images without a well-defined identity-guided mechanism.

VI. ABLATION STUDY

We conduct ablation studies on the proposed DiffUMI and OODD using the LFW [35] and ImageNet [38] datasets, with the privacy-preserving PartialFace [6] model as the target. Type II accuracy is averaged across all four face recognition models for joint evaluation, as outlined in Sec. IV. In each study, we vary a single parameter while holding all others constant to isolate its impact on performance, with parameter settings provided in Tab. II.

A. Model Inversion (DiffUMI)

Reliability of Latent Codes. We propose a latent code generation strategy in Sec. II-D that combines D’Agostino’s K^2 test [40], [41], [42] with MTCNN [43] to improve latent code reliability. As shown in Tab. VI, our approach achieves the highest latent code reliability, leading to superior performance.

Top N Selection. As detailed in Sec. II-E, DiffUMI does not necessitate processing all latent codes. While optimal initialization typically improves reconstruction accuracy, it does not always yield the best results after manipulation. Consequently, we adopt a top N selection strategy, where increasing N enhances reconstruction accuracy at the expense of higher computational cost. Based on our evaluation, we recommend $N = 3$ as an optimal trade-off, achieving strong attack performance with manageable computational overhead, as shown in Tab. VII.

Ranked Adversary. We propose the Ranked Adversary strategy in Sec. II-F to efficiently identify a satisfactory, rather than optimal, solution for model inversion. By prioritizing sequential initialization and allowing early termination once a predefined condition is met, this strategy reduces unnecessary computations. As shown in Tab. VIII, it significantly lowers computational cost with only a minor trade-off in Type II accuracy and OODD performance, effectively balancing efficiency and attack performance.

TABLE VIII

PERFORMANCE (%) WITH AND WITHOUT THE RANKED ADVERSARY STRATEGY. “NO” INDICATES THAT ALL SELECTED N LATENT CODES ARE PROCESSED, AND THE RECONSTRUCTION WITH THE HIGHEST SIMILARITY IS SELECTED AS THE FINAL OUTPUT.

Ranked	Time (s) ↓	Type II (%) ↑	OODD (%) ↓
✓	256	84.42	1.4
✗	530	85.31	1.0

Bold indicates the highest performance, demonstrating that the proposed ranked adversary marginally reduces attack accuracy while significantly enhancing time efficiency.

TABLE IX
PERFORMANCE (%) ACROSS VARYING ATTACK THRESHOLD τ_A .

Threshold τ_A	Time (s) ↓	Similarity ↑	Type II (%) ↑	OODD (%) ↓
0.97	213	0.9712	84.23	1.9
0.98	256	0.9794	84.42	1.4
0.99	442	0.9861	84.98	1.8

Bold indicates the highest performance, showing that increasing τ_A enhances Type II accuracy but substantially raises computational cost and the risk of OODD.

Attack Threshold. We define the attack threshold τ_A in Sec. II-F1 as the criterion for successful manipulation, where the reconstructed image achieves sufficient similarity to the target. This threshold also serves as the early termination criterion in the ranked adversary strategy. τ_A must satisfy $\tau_A \gg \tau_F$ for robustness. However, excessively high values of τ_A (e.g., $\tau_A = 1$) lead to unnecessary computational cost and the risk of overfitting.

For the target model, PartialFace [6], used in this ablation study, the maximum embedding similarity achievable by real facial images is 0.98. As shown in Tab. IX, $\tau_A < 0.98$ results in faster model inversion completion, whereas $\tau_A > 0.98$ improves Type II accuracy at the cost of increased computational overhead. Additionally, higher τ_A values increase the risk of being detected as out-of-domain due to greater distortion in the reconstructed images. These results demonstrate that our proposed strategy (Sec. II-F1), which defines τ_A as the maximum embedding similarity achievable by real facial images in the target model, is optimal.

Perturbation Constraint. As discussed in Fig. 4, the L_2 -norm constrained adversary better preserves normality compared to the L_∞ -norm adversary, leading to improved reconstruction fidelity. This is further validated by Tab. X, where L_2 -norm ($\epsilon = 35$) and L_∞ -norm ($\epsilon = 0.15$) achieve similar similarity values, yet the L_2 -norm attack demonstrates significantly superior performance. Additionally, Tab. X and Fig. 12 show that while increasing the attack magnitude ϵ enhances Type II accuracy and accelerates the attack, it also introduces more artifacts, raising the likelihood of detection as out-of-domain inputs.

B. Out-of-Domain Detection (OODD)

We propose OODD framework in Sec. III, integrating two failure cases: matching failure and face detection failure. Both

TABLE X
PERFORMANCE (%) UNDER VARYING PERTURBATION CONSTRAINTS.

Norm	Magnitude ϵ	Time(s)↓	Similarity↑	Type II(%)↑	OODD(%)↓
L_2	30	455	0.9707	81.49	1.5
L_2	35	256	0.9794	84.42	1.4
L_2	40	191	0.9816	86.11	3.2
L_∞	0.15	260	0.9791	75.28	3.1

Bold denotes the highest performance, indicating that the L_2 -norm constraint yields the best results. Increasing ϵ accelerates the attack and improves Type II accuracy, but also introduces more noise, increasing the risk of OODD.

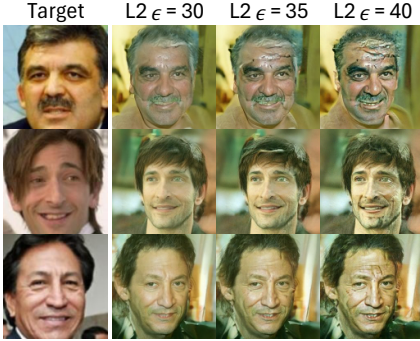


Fig. 12. Larger perturbation magnitudes lead to increased distortion due to more pronounced noise and diminished naturalness in the generation.

TABLE XI
OODD RATE (%) WHEN JOINTLY CONSIDERING BOTH FAILURE CASES (OURS) VERSUS INDIVIDUAL STRATEGIES.

Target Model	Dataset	Matching Failure	Detection Failure	Ours
FaceNet	CelebA	0.6	1.7	2.3
	LFW	3.4	1.7	4.9
	ImageNet	49.6	57.9	91.3
ArcFace	CelebA	0.0	4.4	4.4
	LFW	0.2	3.2	3.4
	ImageNet	1.6	98.4	98.9
DCTDP	CelebA	0.0	4.9	4.9
	LFW	0.2	3.6	3.7
	ImageNet	20.9	81.6	95.5
PartialFace	CelebA	0.1	1.6	1.7
	LFW	0.8	0.6	1.4
	ImageNet	55.3	57.0	95.2

Red indicates instances of failed detection (insufficient detection rates), highlighting the superiority of our joint strategy over individual strategies.

criteria must be considered together, as relying on a single strategy alone is insufficient for effective OODD. As shown in Tab. XI (see red values), using only one strategy results in an OODD rate of approximately 50% for out-of-domain inputs (*i.e.*, ImageNet), highlighting its limitations.

VII. DISCUSSION ON DEFENSES AGAINST DIFFUMI

We have demonstrated the success of our attack on two methods designed to mitigate model inversion by reducing facial information exposure, either through randomization of frequency components or by managing privacy budgets [5], [6]. However, more advanced strategies, such as feder-

ated learning, aim to counter privacy recovery. Investigating whether our method can generalize to these broader defense strategies represents a valuable extension of our work.

Nevertheless, the core strategy of our model inversion attack is to refine facial reconstruction while minimizing artifacts to avoid overfitting to the target model. We argue that if a facial image can match the target embedding without overfitting due to artifacts, it must correspond to the correct identity. This optimization approach relies solely on the input and output of the target model, which cannot bypass in an application context. Therefore, we believe our model inversion attack should be effective against any target system providing input-output access, regardless of integrated defense mechanisms.

We posit that the most efficient defense against our attack would involve hiding gradients to prevent white-box model inversion. However, while our black-box version is computationally more intensive, it is not impossible to execute, though it requires significantly more time. We acknowledge this as a limitation and note that further testing is needed to verify these discussions in future work.

VIII. CONCLUSION, LIMITATION, AND FUTURE WORK

In this paper, we introduce DiffUMI, the first approach to leverage diffusion models for unconditional facial image generation, achieving a training-free model inversion attack for open-set face recognition models. This eliminates the need for training separate generators for different models, addressing a key limitation of previous methods. Additionally, we propose OODD, a novel out-of-domain input detection framework that operates solely on feature embeddings. Our results demonstrate that DiffUMI achieves state-of-the-art performance in model inversion attacks, making it a powerful tool for evaluating the privacy vulnerabilities of face recognition models. Moreover, we are the first to systematically analyze the impact of latent code reliability on generation fidelity and propose an automated method for selecting highly reliable latent codes. We also provide new insights into the most effective adversarial attack strategies for manipulating latent space, rather than focusing on specific attack algorithms.

Despite these contributions, we acknowledge three limitations. First, the computational cost of black-box DiffUMI remains prohibitively high, limiting its practical deployment. Second, modifying latent codes without introducing significant artifacts using diffusion-driven unconditional image generation presents a fundamental challenge, restricting the extent of feasible modifications. Third, further investigation is needed to uncover the mathematical reasons behind the poor performance of coarse-grained adversarial manipulation in unconditional image generation.

For future work, beyond addressing the aforementioned limitations, we aim to extend DiffUMI to broader domains, including classification models for datasets such as CIFAR-10, ImageNet, and medical imaging. Additionally, we intend to evaluate the potential defenses against our model inversion attack, as outlined in Sec. VII. We also plan to develop objective evaluation metrics to replace human assessment, as

subjective judgments, such as “Do these two images belong to the same person?”, are inherently inconsistent.

In extending ODD, we would like to investigate its potential applications in data poisoning detection and defense against malicious inputs. Additionally, we consider developing a novel ODD framework independent of model inversion to enhance its applicability and robustness.

REFERENCES

- [1] Microsoft, *Face API Reference*, 2024. Azure AI Services Documentation.
- [2] A. W. Services, *Amazon Rekognition Documentation*, 2024. AWS Documentation.
- [3] G. Cloud, *Cloud Vision Documentation*, 2024. Google Cloud Documentation.
- [4] Face++, *Face++ Documentation*, 2024. Face++ Official Documentation.
- [5] J. Ji, H. Wang, Y. Huang, J. Wu, X. Xu, S. Ding, S. Zhang, L. Cao, and R. Ji, “Privacy-preserving face recognition with learnable privacy budgets in frequency domain,” in *European Conference on Computer Vision (ECCV)*, (Tel Aviv, Israel), pp. 475–491, Springer, 2022.
- [6] Y. Mi, Y. Huang, J. Ji, M. Zhao, J. Wu, X. Xu, S. Ding, and S. Zhou, “Privacy-preserving face recognition using random frequency components,” in *Proceedings of the IEEE/CVF International Conference on Computer Vision (ICCV)*, (Paris, France), pp. 19673–19684, IEEE, 2023.
- [7] Z. Boulkenafet, J. Komulainen, L. Li, X. Feng, and A. Hadid, “Oulu-npu: A mobile face presentation attack database with real-world variations,” in *2017 12th IEEE international conference on automatic face & gesture recognition (FG 2017)*, pp. 612–618, IEEE, 2017.
- [8] H. Zhang, X. Dong, Y. Lai, Y. Zhou, X. Zhang, X. Lv, Z. Jin, and X. Li, “Validating privacy-preserving face recognition under a minimum assumption,” in *Proceedings of the IEEE/CVF Conference on Computer Vision and Pattern Recognition (CVPR)*, (Seattle, Washington, United States), pp. 12205–12214, IEEE, 2024.
- [9] M. Fredrikson, S. Jha, and T. Ristenpart, “Model inversion attacks that exploit confidence information and basic countermeasures,” in *Proceedings of the 22nd ACM SIGSAC Conference on Computer and Communications Security (ACM CCS)*, pp. 1322–1333, 2015.
- [10] G. Mai, K. Cao, P. C. Yuen, and A. K. Jain, “On the reconstruction of face images from deep face templates,” *IEEE Transactions on Pattern Analysis and Machine Intelligence*, vol. 41, no. 5, pp. 1188–1202, 2018.
- [11] Z. Zhang, X. Wang, J. Huang, and S. Zhang, “Analysis and utilization of hidden information in model inversion attacks,” *IEEE Transactions on Information Forensics and Security*, 2023.
- [12] H. O. Shahreza, V. K. Hahn, and S. Marcel, “Vulnerability of state-of-the-art face recognition models to template inversion attack,” *IEEE Transactions on Information Forensics and Security*, 2024.
- [13] C. N. Duong, T.-D. Truong, K. Luu, K. G. Quach, H. Bui, and K. Roy, “Vec2face: Unveil human faces from their blackbox features in face recognition,” in *Proceedings of the IEEE/CVF Conference on Computer Vision and Pattern Recognition (CVPR)*, pp. 6132–6141, 2020.
- [14] Y. Zhang, R. Jia, H. Pei, W. Wang, B. Li, and D. Song, “The secret revealer: Generative model-inversion attacks against deep neural networks,” in *Proceedings of the IEEE/CVF Conference on Computer Vision and Pattern Recognition (CVPR)*, pp. 253–261, 2020.
- [15] M. Khosravy, K. Nakamura, Y. Hirose, N. Nitta, and N. Babaguchi, “Model inversion attack by integration of deep generative models: Privacy-sensitive face generation from a face recognition system,” *IEEE Transactions on Information Forensics and Security*, vol. 17, pp. 357–372, 2022.
- [16] X. Yuan, K. Chen, J. Zhang, W. Zhang, N. Yu, and Y. Zhang, “Pseudo label-guided model inversion attack via conditional generative adversarial network,” in *Proceedings of the AAAI Conference on Artificial Intelligence (AAAI)*, vol. 37, pp. 3349–3357, 2023.
- [17] B.-N. Nguyen, K. Chandrasegaran, M. Abdollahzadeh, and N.-M. M. Cheung, “Label-only model inversion attacks via knowledge transfer,” *Advances in Neural Information Processing Systems (NIPS)*, vol. 36, 2023.
- [18] J. Wu, C. Wan, H. Chen, Z. Zheng, and Y. Sun, “Label-only model inversion attacks: Adaptive boundary exclusion for limited queries,” *Neurocomputing*, p. 129902, 2025.
- [19] M. Kansy, A. Raël, G. Mignone, J. Naruniec, C. Schroers, M. Gross, and R. M. Weber, “Controllable inversion of black-box face recognition models via diffusion,” in *Proceedings of the IEEE/CVF International Conference on Computer Vision (ICCV) Workshops*, pp. 3167–3177, 2023.
- [20] R. Liu, D. Wang, Y. Ren, Z. Wang, K. Guo, Q. Qin, and X. Liu, “Unstoppable attack: Label-only model inversion via conditional diffusion model,” *IEEE Transactions on Information Forensics and Security*, 2024.
- [21] H. Otrosi Shahreza and S. Marcel, “Face reconstruction from facial templates by learning latent space of a generator network,” *Advances in Neural Information Processing Systems (NIPS)*, vol. 36, 2023.
- [22] H. O. Shahreza and S. Marcel, “Template inversion attack using synthetic face images against real face recognition systems,” *IEEE Transactions on Biometrics, Behavior, and Identity Science*, 2024.
- [23] L. Struppek, D. Hintersdorf, A. D. A. Correia, A. Adler, and K. Kersting, “Plug & play attacks: Towards robust and flexible model inversion attacks,” in *International Conference on Machine Learning (ICML)*, pp. 20522–20545, PMLR, 2022.
- [24] Y. Qiu, H. Fang, H. Yu, B. Chen, M. Qiu, and S.-T. Xia, “A closer look at gan priors: Exploiting intermediate features for enhanced model inversion attacks,” in *European Conference on Computer Vision (ECCV)*, pp. 109–126, Springer, 2024.
- [25] X. Dong, Z. Miao, L. Ma, J. Shen, Z. Jin, Z. Guo, and A. B. J. Teoh, “Reconstruct face from features based on genetic algorithm using gan generator as a distribution constraint,” *Computers & Security*, vol. 125, p. 103026, 2023.
- [26] S. Pang, Y. Rao, Z. Lu, H. Wang, Y. Zhou, and M. Xue, “Pridm: Effective and universal private data recovery via diffusion models,” *IEEE Transactions on Dependable and Secure Computing*, 2025.
- [27] R. Rombach, A. Blattmann, D. Lorenz, P. Esser, and B. Ommer, “High-resolution image synthesis with latent diffusion models,” in *Proceedings of the IEEE/CVF Conference on Computer Vision and Pattern Recognition (CVPR)*, pp. 10684–10695, 2022.
- [28] I. Goodfellow, J. Pouget-Abadie, M. Mirza, B. Xu, D. Warde-Farley, S. Ozair, A. Courville, and Y. Bengio, “Generative adversarial nets,” *Advances in neural information processing systems (NIPS)*, vol. 27, 2014.
- [29] A. Radford, L. Metz, and S. Chintala, “Unsupervised representation learning with deep convolutional generative adversarial networks,” in *International Conference on Learning Representations (ICLR)*, 2016.
- [30] T. Karras, S. Laine, M. Aittala, J. Hellsten, J. Lehtinen, and T. Aila, “Analyzing and improving the image quality of stylegan,” in *Proceedings of the IEEE/CVF Conference on Computer Vision and Pattern Recognition (CVPR)*, pp. 8110–8119, 2020.
- [31] C. Meng, Y. He, Y. Song, J. Song, J. Wu, J.-Y. Zhu, and S. Ermon, “SDEdit: Guided image synthesis and editing with stochastic differential equations,” in *International Conference on Learning Representations (ICLR)*, 2022.
- [32] F. Croce and M. Hein, “Reliable evaluation of adversarial robustness with an ensemble of diverse parameter-free attacks,” in *International Conference on Machine Learning (ICML)*, pp. 2206–2216, 2020.
- [33] H. Wang, C.-C. Chang, C.-S. Lu, C. Leckie, and I. Echizen, “Greedy-pixel: Fine-grained black-box adversarial attack via greedy algorithm,” *arXiv preprint arXiv:2501.14230*, 2025.
- [34] C.-H. Lee, Z. Liu, L. Wu, and P. Luo, “Maskgan: Towards diverse and interactive facial image manipulation,” in *IEEE Conference on Computer Vision and Pattern Recognition (CVPR)*, 2020.
- [35] G. B. Huang, M. Mattar, T. Berg, and E. Learned-Miller, “Labeled faces in the wild: A database for studying face recognition in unconstrained environments,” in *Workshop on Faces in 'Real-Life' Images: Detection, Alignment, and Recognition*, 2008.
- [36] F. Schroff, D. Kalenichenko, and J. Philbin, “Facenet: A unified embedding for face recognition and clustering,” in *Proceedings of the IEEE Conference on Computer Vision and Pattern Recognition (CVPR)*, (Boston, Massachusetts, USA), pp. 815–823, IEEE, 2015.
- [37] J. Deng, J. Guo, N. Xue, and S. Zafeiriou, “Arcface: Additive angular margin loss for deep face recognition,” in *Proceedings of the IEEE/CVF Conference on Computer Vision and Pattern Recognition (CVPR)*, (Long Beach, CA, USA), pp. 4690–4699, IEEE, 2019.
- [38] I. G. Alex K, Ben Hamner, “Nips 2017: Defense against adversarial attack,” 2017.
- [39] J. Ho, A. Jain, and P. Abbeel, “Denoising diffusion probabilistic models,” *Advances in neural information processing systems*, vol. 33, pp. 6840–6851, 2020.

- [40] R. B. D’Agostino, “Transformation to normality of the null distribution of g_1 ,” *Biometrika*, vol. 57, no. 3, pp. 679–681, 1970.
- [41] R. D’agostino and E. S. Pearson, “Tests for departure from normality. empirical results for the distributions of b^2 and $\sqrt{b^1}$,” *Biometrika*, vol. 60, no. 3, pp. 613–622, 1973.
- [42] R. B. D’agostino, A. Belanger, and R. B. D’Agostino Jr, “A suggestion for using powerful and informative tests of normality,” *The American Statistician*, vol. 44, no. 4, pp. 316–321, 1990.
- [43] K. Zhang, Z. Zhang, Z. Li, and Y. Qiao, “Joint face detection and alignment using multitask cascaded convolutional networks,” *IEEE Signal Processing Letters*, vol. 23, no. 10, pp. 1499–1503, 2016.
- [44] M. Andriushchenko, F. Croce, N. Flammarion, and M. Hein, “Square attack: a query-efficient black-box adversarial attack via random search,” in *European Conference on Computer Vision (ECCV)*, pp. 484–501, 2020.
- [45] Q. V. Vo, E. Abbasnejad, and D. Ranasinghe, “Brusleattack: Query-efficient score-based sparse adversarial attack,” in *The Twelfth International Conference on Learning Representations (ICLR)*, 2024.
- [46] T. Karras, S. Laine, and T. Aila, “A style-based generator architecture for generative adversarial networks,” in *Proceedings of the IEEE/CVF Conference on Computer Vision and Pattern Recognition (CVPR)*, pp. 4401–4410, 2019.
- [47] Q. Cao, L. Shen, W. Xie, O. M. Parkhi, and A. Zisserman, “Vggface2: A dataset for recognising faces across pose and age,” in *2018 13th IEEE International Conference on Automatic Face & Gesture Recognition (FG 2018)*, pp. 67–74, IEEE, 2018.
- [48] Y. Guo, L. Zhang, Y. Hu, X. He, and J. Gao, “Ms-celeb-1m: A dataset and benchmark for large-scale face recognition,” in *14th European Conference on Computer Vision (ECCV)*, pp. 87–102, Springer, 2016.
- [49] A. Krizhevsky, G. Hinton, *et al.*, “Learning multiple layers of features from tiny images,” tech. rep., University of Toronto, 2009.
- [50] Y. Song, J. Sohl-Dickstein, D. P. Kingma, A. Kumar, S. Ermon, and B. Poole, “Score-based generative modeling through stochastic differential equations,” in *International Conference on Learning Representations (ICLR)*, 2021.
- [51] P. Dhariwal and A. Nichol, “Diffusion models beat gans on image synthesis,” *Advances in Neural Information Processing Systems (NIPS)*, vol. 34, pp. 8780–8794, 2021.

APPENDIX

A. Benchmarking Against Training-Dependent Methods

As shown in Tab. I, MAP²V [8] is the most recent and relevant state-of-the-art baseline, sharing our training-free approach and focus on open-set face recognition. In this section, we additionally compare with training-dependent attacks [22], [12], as summarized in Tab. XII and Fig. 13. These two methods are not our primary baselines due to a critical limitation: each target model requires a separately trained generator, incurring significant computational cost. We exclude closed-set face recognition attacks, as they depend on class labels rather than target embeddings, and therefore operate under fundamentally different assumptions.

As shown in Tab. XII, we evaluate two training-dependent attacks [22], [12], each involving a generator trained specifically for the target model ArcFace [37]. Notably, the training dataset (FFHQ [46]) differs from the testing set (LFW [35]), ensuring an open-set evaluation. In contrast, both MAP²V [8] and our proposed DiffUMI are training-free. This setup inherently favors training-dependent methods; nevertheless, DiffUMI achieves performance comparable to DSCasConv [12], while significantly outperforming the other two baselines.

Despite DSCasConv’s strong reconstruction accuracy, it faces substantial limitations. Specifically, it took 1.5 days of training on dual A100 80GB GPUs and is constrained to generating 112×112 resolution images for a specific

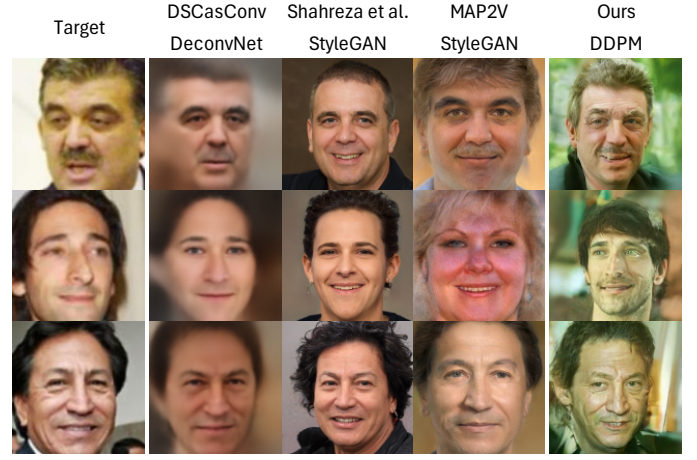


Fig. 13. Visual fidelity comparison of reconstruction results across different attack methods. Both Shahreza *et al.* [22] and our method achieve high-resolution, headshot-style reconstructions with superior visual quality. In contrast, DSCasConv [12] yields the lowest fidelity, characterized by lowest resolution, blurred features, and limited facial detail.

target model. Moreover, as illustrated in Fig. 13, DSCasConv produces the lowest visual fidelity, with blurred features and limited facial detail. These limitations highlight the importance of training-free approaches and underscore the advantages of leveraging generative models such as GANs or diffusion models.

B. Preliminary

1) *Image Generation via DDPM*: Denoising Diffusion Probabilistic Models (DDPM) [39] are generative models that refine images by reversing a diffusion process. Pretrained DDPMs have been applied to unconditional image generation of faces [31], CIFAR-10 [49], [50], and ImageNet [38], [51] from Gaussian distributions. In the forward diffusion process, Gaussian noise is progressively added to a data sample x_0 over T time steps, generating a sequence $\{x_t\}_{t=1}^T$.

$$q(x_t | x_{t-1}) = \mathcal{N}(x_t; \sqrt{\alpha_t}x_{t-1}, (1 - \alpha_t)I), \quad (23)$$

where $\alpha_t = 1 - \beta_t$ and β_t is a predefined noise variance schedule. The marginal distribution of x_t is given by:

$$q(x_t | x_0) = \mathcal{N}(x_t; \sqrt{\bar{\alpha}_t}x_0, (1 - \bar{\alpha}_t)I), \quad (24)$$

where $\bar{\alpha}_t = \prod_{s=1}^t \alpha_s$. The reverse process aims to denoise $x_T \sim \mathcal{N}(0, I)$ back to a realistic image x_0 using a learned model p_θ :

$$p_\theta(x_{t-1} | x_t) = \mathcal{N}(x_{t-1}; \mu_\theta(x_t, t), \Sigma_\theta(x_t, t)). \quad (25)$$

For image generation, the pretrained DDPM learns a denoising function ϵ_θ , parameterized by a neural network:

$$\epsilon_\theta(x_t, t) \approx \epsilon \sim \mathcal{N}(0, I), \quad (26)$$

optimized through the objective:

$$\mathcal{L}_{\text{DDPM}} = \mathbb{E}_{x_0, \epsilon, t} [\|\epsilon - \epsilon_\theta(x_t, t)\|^2]. \quad (27)$$

TABLE XII
COMPARISON OF DIFFUMI WITH BENCHMARK ATTACK METHODS.

Attack	Generator	Training-Free	Dataset	Target Model	Test Model									
					FaceNet		ArcFace		DCTDP		PartialFace		Avg.	
					Type I	Type II	Type I	Type II	Type I	Type II	Type I	Type II	Type I	Type II
DSCasConv [12]	DeconvNet	✗	LFW	ArcFace	97.10	90.42	100.00	99.03	99.90	97.16	99.50	93.21	99.13	94.96
Shahreza <i>et al.</i> [22]	StyleGAN	✗			61.00	49.33	98.10	77.79	84.10	59.41	74.00	52.24	79.30	59.69
MAP ² V [8]	StyleGAN	✓			67.60	60.40	100.00	99.42	97.10	83.78	91.20	73.27	88.98	79.22
Ours	DDPM	✓			96.00	91.03	100.00	99.64	99.60	95.88	98.60	92.33	98.55	94.72

Gray cells indicate cases where the target and test models are identical. Our training-free attack achieves performance comparable to the training-dependent DSCasConv attack, while significantly outperforming the other two baselines.

TABLE XIII
KEY NOTATIONS AND THEIR CORRESPONDING DEFINITIONS.

Notation	Definition	Remark	Reference
$F(\cdot)$	Embedding function (Face recognition)		
x^T	Target facial image	Unknown to Attackers	
z^T	Target embedding, transformed from the target face	Known to Attackers	
\hat{x}	Reconstructed image	Attack Output	
\hat{z}	Feature embedding of the reconstructed image		
$G(\cdot)$	Generative function (DDPM)	Pretrained	
x_G	Latent code, drawn from a random Gaussian distribution	Attack Input	Sec. II-C
x'_G	Manipulated latent code		
δ	Adversarial perturbations on the latent code		
$\ \cdot\ _p$	L_p -norm		
ϵ	Perturbation magnitude	Attack Setting	
$S(\cdot, \cdot)$	Similarity function (cosine)		
\mathcal{L}	Objective function		
τ_F	Similarity decision threshold		
$K(\cdot)$	Gaussian normality test function (K^2 test)		
p_K	Gaussian normality (the probability of following a normal distribution)		Sec. II-D1
τ_K	Threshold of Gaussian normality	Attack Setting	
$D(\cdot)$	Face detection function (MTCNN)		
p_D	Face detection confidence score		Sec. II-D2
τ_D	Threshold of detection confidence	Attack Setting	
V	Volume of reliable latent codes (Step (a))	Attack Setting	
N	Top N selection (Step (b))	Attack Setting	Sec. II-E
Q	Query Efficiency		
t_{max}	Maximum iterations per adversarial attack	Attack Setting	
Q_{max}	Maximum number of queries (only for black-box attacks)	Attack Setting	
τ_A	Attack threshold (sufficient similarity)	Attack Setting	Sec. II-F
$\lfloor \cdot \rfloor$	Floor function		
$\mathbb{I}(\cdot)$	Indicator function		
I	Total number of attack samples		Sec. IV
$x^{j \neq T}$	Facial images distinct from the target, associated with the same identity		
J	Total number of $x^{j \neq T}$ for each identity		

This noise-aware iterative refinement process enables high-fidelity image generation.

We define the final denoised image x_0 as the reconstructed image \hat{x} , generated by applying a pretrained DDPM as a generative function $G(\cdot)$ to an initial Gaussian noise sample x_G :

$$\hat{x} = G(x_G). \quad (28)$$

Here, x_G acts as a latent code sampled from a Gaussian distribution, which $G(\cdot)$ iteratively refines into a high-fidelity image \hat{x} .

2) *Open-Set Face Recognition*: Open-set face recognition systems [36], [37], [5], [6] map facial images to feature embeddings, classifying an image pair as the same identity if their embedding similarity exceeds a predefined threshold. This threshold is typically set to balance the false positive rate or achieve the minimum equal error rate.

Let $F(\cdot)$ be the embedding function of a face recognition model that maps a facial image x to a d -dimensional feature embedding z , encoding identity-specific attributes while ensuring robustness to variations in lighting, pose, and expression.

Formally:

$$z = F(x), \quad z \in \mathbb{R}^d, \quad (29)$$

where d is determined by the model's architecture and training process.

Feature embeddings facilitate identity verification or recognition by measuring similarity using metrics such as cosine similarity or Euclidean distance. Given two embeddings, $z_1 = F(x_1)$ and $z_2 = F(x_2)$, their similarity score is computed as:

$$S(z_1, z_2) = \frac{z_1 \cdot z_2}{\|z_1\| \|z_2\|}, \quad (30)$$

for cosine similarity. If $S(z_1, z_2) \geq \tau_F$, the images are classified as belonging to the same identity. In this work, τ_F denotes the predefined similarity threshold set at the minimum equal error rate.

3) *D'Agostino's K-Square Test*: Given a randomly generated latent code x_G , the K^2 test function $K(\cdot)$ [40], [41], [42] quantifies deviations from normality based on skewness and kurtosis, producing a probability value:

$$p_K = K(x_G) = 1 - \Psi_2(Y_1^2 + Y_2^2), \quad (31)$$

where Y_1 and Y_2 are the standardized skewness and kurtosis statistics:

$$Y_1 = \frac{b_1 - \mu_1}{\sigma_1}, \quad Y_2 = \frac{b_2 - \mu_2}{\sigma_2}. \quad (32)$$

Here, b_1 and b_2 represent the sample skewness and excess kurtosis, while μ_1, σ_1, μ_2 , and σ_2 denote their respective means and standard deviations under normality. The function $\Psi_2(\cdot)$ is the cumulative distribution function of the chi-squared distribution with two degrees of freedom.

4) *Face Detection via MTCNN*: Multi-Task Cascaded Convolutional Neural Networks (MTCNN) [43] uses a three-stage cascaded architecture: (i) The Proposal Network (P-Net) scans the image across multiple scales to generate candidate face regions. (ii) The Refinement Network (R-Net) filters false positives and refines bounding boxes. (iii) The Output Network (O-Net) further refines detections and predicts five facial landmarks. The final detection confidence is obtained through:

$$p_D = D(\hat{x}) = f_{\text{O-Net}}(f_{\text{R-Net}}(f_{\text{P-Net}}(\hat{x}))). \quad (33)$$

C. Notations and Definitions

The key notations and their corresponding definitions are summarized in Tab. XIII. Less significant notations, not directly relevant to the proposed methodologies, are omitted from this list.

D. Algorithms of DiffUMI

The step-by-step algorithm of the proposed model inversion attack, DiffUMI, is detailed in Figs. 14 to 16.

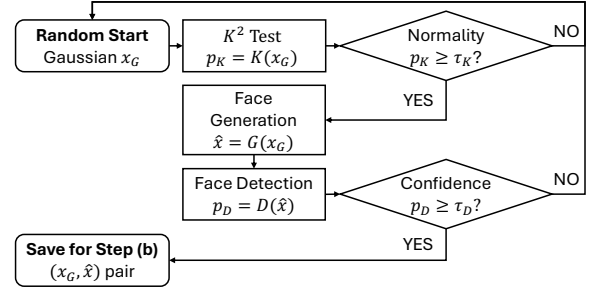


Fig. 14. The algorithm of the proposed two-stage latent code generation process. Initially, D'Agostino's K^2 test $K(\cdot)$ [40], [41], [42] evaluates a randomly generated latent code x_G , retaining those that exhibit Gaussian normality with a p_K value exceeding the threshold τ_K . Subsequently, MTCNN $D(\cdot)$ [43] assesses whether the latent code can generate a facial image \hat{x} , with face detection confidence p_D surpassing the threshold τ_D .

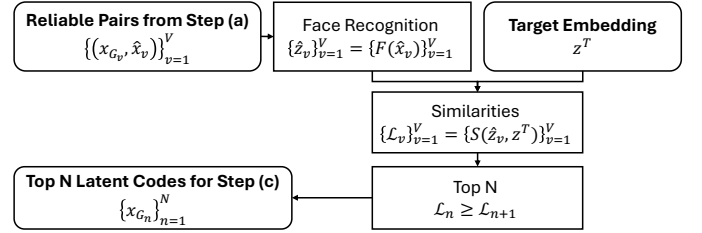


Fig. 15. Algorithm for selecting the top N latent codes based on the highest embedding similarity between their reconstructions and the target.

E. More Results in Terms of Type I Accuracy

In Sec. IV, we introduce Type I and Type II accuracy as metrics for assessing the effectiveness of privacy attacks. This study primarily focuses on Type II accuracy, which quantifies the similarity between reconstructed facial images and images from the target identity, excluding the target image itself. Type II accuracy offers a more rigorous evaluation by mitigating the risk of overfitting to the target image, whose embedding is used as a reference during the attack. For further validation, we also report Type I accuracy results, which reflect the strength of the inversion attack and highlight potential privacy vulnerabilities. Specifically, Type I accuracy is the rate at which the reconstructed image \hat{x} matches the target face x^T in the feature space of the face recognition model $F(\cdot)$:

$$\text{Type I Accuracy} = \frac{\sum_{i=1}^I \mathbb{I}(S(F(\hat{x}_i), F(x_i^T)) \geq \tau_F)}{I}, \quad (34)$$

where $\mathbb{I}(\cdot)$ and $S(\cdot, \cdot)$ represent the indicator and cosine similarity functions, respectively. I is the total number of attack samples, and τ_F is the similarity threshold for face recognition.

The results in Tabs. XIV and XV reinforce our main paper's conclusion that all tested face recognition models are vulnerable to our privacy attack. Among them, FaceNet, the oldest standard model, exhibits the highest resistance, underscoring the limitations of existing privacy-preserving techniques. Our approach consistently outperforms the benchmark MAP²V at-

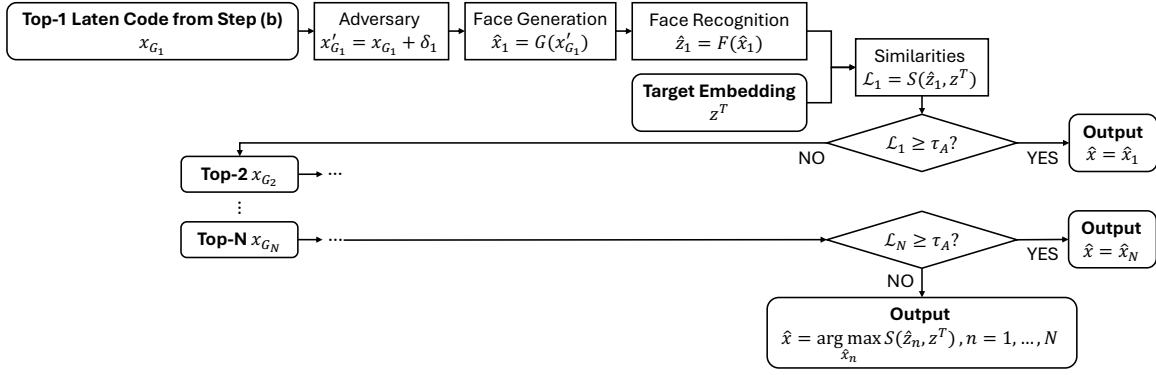


Fig. 16. Algorithm for the proposed Ranked Adversary in latent code manipulation. This process sequentially optimizes the top N initial latent codes, ranked in Step (b), through adversarial manipulation to achieve the objective defined in Eq. (7) using the objective function in Eq. (6). The process concludes once $\mathcal{L}_n \geq \tau_A$, $n = 1, \dots, N$ for any manipulated latent code. If no code meets this criterion, the reconstruction with the highest \mathcal{L}_n is selected as the final output.

TABLE XIV
TYPE I ACCURACY (%) OF DIFFUMI ACROSS FOUR FACE RECOGNITION MODELS.

Dataset	Target Model	FaceNet	Test Model			Avg.
			ArcFace	DCTDP	PartialFace	
CelebA	FaceNet	100.0	96.7	97.9	94.9	97.38
	ArcFace	99.9	100.0	100.0	99.9	99.95
	DCTDP	99.3	99.5	100.0	99.9	99.68
	PartialFace	97.7	99.2	99.6	100.0	99.13
LFW	FaceNet	100.0	87.0	93.4	80.8	90.30
	ArcFace	96.0	100.0	99.6	98.6	98.55
	DCTDP	96.7	99.7	100.0	97.8	98.55
	PartialFace	90.9	98.7	96.2	100.0	96.45

Gray cells indicate cases where the target and test models are identical. Green and Red highlight the most and least secure models, respectively, based on the lowest and highest Type I accuracy.

tack [8], achieving higher Type I accuracy across all scenarios. Notably, Type I accuracy exceeds Type II accuracy by 3.83% to 15.79%, demonstrating that our primary evaluation metric is more rigorous and comprehensive.

TABLE XV
TYPE I ACCURACY (%) OF OUR DIFFUMI ACROSS FOUR FACE RECOGNITION MODELS, COMPARED TO THE BENCHMARK ATTACK MAP²V [8].

Dataset	Attack	FaceNet	Target Model		PartialFace
			ArcFace	DCTDP	
CelebA	Original ¹	100.00	100.00	100.00	100.00
	Random ²	4.40	1.30	4.20	10.10
	MAP ² V	89.75	95.03	96.75	97.98
	Ours	97.38	99.95	99.68	99.13
LFW	Original ¹	100.00	100.00	100.00	100.00
	Random ²	0.70	0.00	0.20	0.50
	MAP ² V	90.05	88.98	92.50	90.54
	Ours	90.30	98.55	98.55	96.45

¹ Upper bound corresponding to true target faces.

² Lower bound referring to randomly generated facial images without a specific strategy.

Bold indicates the highest performance among attack methods, with our approach exceeding the SOTA MAP²V attack by up to 9.57% in Type I accuracy.